

MPI-PhT/2003-09  
TUM-HEP-500/03  
hep-ph/0302244  
May 2003

# Complete 1-Loop Calculation of the T-violating $D$ -Parameter in Neutron Decay in the MSSM

Manuel Drees<sup>1</sup> and Michael Rauch<sup>2</sup>

<sup>1</sup> *Physik Dept. TU München, D-85748 Garching, Germany*

<sup>2</sup> *MPI f. Physik, Föhringer Ring 6, 80805 München, Germany*

## Abstract

We investigate the violation of time reversal invariance in the decay of the free neutron in the framework of the Minimal Supersymmetric Standard Model (MSSM). The coefficient of the triple product of the neutron spin and the momenta of electron and neutrino, the so called  $D$  parameter, is computed at one loop order including all diagrams. We find that  $D$  is mainly sensitive to the trilinear  $A$  coupling in the squark sector and to the phase of the coefficient  $\mu$  which mixes the two Higgs superfields. The maximal MSSM contribution using parameters still allowed by experiment is however at  $D \approx 10^{-7}$ , while QED final state interactions give a value of  $D_{\text{fsi}} = -2.3 \cdot 10^{-5}$ . Explicit expressions for all relevant diagrams are given in an Appendix.

# 1 Introduction

The existence of complex parameters in the Lagrangian can lead to a violation of time reversal symmetry. In the standard model the phase of the CKM matrix is the only phase which cannot be eliminated by a field redefinition. In the MSSM there are additional parameters which in general cannot be made real:

- the coefficient of the term bilinear in the Higgs superfields:  $\mu$
- two of the three gaugino masses  $\tilde{m}_i \quad i = 1, 2$
- terms mixing left- and right-handed sfermions  $A_f$ .

The violation of (naive)  $T$  symmetry can be tested using an observable which is odd under applying the  $T$  symmetry operator. For example an odd combination of spins and momenta fulfills this condition. In this paper we investigate the triple product

$$\frac{\vec{\sigma}_n}{\sigma_n} \cdot (\vec{p}_e \times \vec{p}_{\bar{\nu}}) \quad (1)$$

of the spin of the neutron and the momenta of electron and electron antineutrino in the decay of free neutrons. The coefficient of this expression in the decay distribution

$$\frac{d\Gamma}{dE_e d \cos \theta_{e\bar{\nu}}} = G_e(E_e) \left\{ 1 + D \frac{\vec{\sigma}_n \cdot \vec{p}_e \times \vec{p}_{\bar{\nu}}}{\sigma_n E_e E_{\bar{\nu}}} + \dots \right\} \quad (2)$$

where  $G_e$  is the tree level expression, is called the  $D$  parameter. It offers a distinct possibility to search for  $T$  symmetry violation in neutron decay, besides the electric dipole moment of the neutron. An experimental effort is currently underway at the ILL Grenoble to improve the measurement of, or bound on,  $D$ . A complete calculation of  $D$  in the MSSM therefore seems timely. To the best of our knowledge, only the gluino loop contribution to  $D$  has previously been calculated [1].

In this paper we follow the conventions of Rosiek [2]; that reference also contains expressions for all relevant Feynman rules. A brief summary of the (somewhat unusual) notation is given in Appendix A.

## 2 $D$ –Parameter

### 2.1 Standard Model

As remarked earlier, the only  $T$ –violating parameter in the Standard Model (SM) is the phase in the Kobayashi–Maskawa matrix. It can lead to violation of  $T$  (or  $CP$ ) symmetry only in processes involving all three generations of quarks. Therefore it can contribute to the  $D$ –parameter only starting at the two–loop level. As a result, the truly  $T$  symmetry violating contribution to  $D$  is very small in the SM [3],

$$D_{SM} \leq 10^{-12}. \quad (3)$$

Experimentally a complete time reversal, which would consist of motion reversal *and* exchange of the initial and final states, is unfortunately not possible in neutron decay. Instead,

$D$  is odd under so-called naive time reversal, where only the directions of all spin and momentum three-vectors are reversed, without exchanging initial and final state [4]. While genuine  $T$  invariance can only be violated if some parameters in the fundamental Lagrangian contain nontrivial complex phases, naive time reversal invariance can be violated whenever the relevant matrix element has a nonvanishing imaginary part. This difference is significant, since an imaginary part in the matrix element, a so-called absorptive phase, can also originate from loop corrections which respect genuine  $T$  invariance. In the present case these are due to QED final state interactions between the proton and the electron. Note that a loop diagram gives an absorptive phase only if the particles in the loop can be on-shell; this leads to an additional phase space suppression factor of order  $E_e/m_n$ , where  $m_n$  is the neutron mass and  $E_e$  the energy of the electron in the neutron rest frame. The total contribution from final state interactions is therefore quite small [5],

$$|D_{\text{fsi}}| \leq 2.3 \cdot 10^{-5}; \quad (4)$$

the bound is saturated at the kinematic maximum of  $E_e$ . “New physics” contributions to  $D$  that are much smaller than this value will be very difficult to extract even for arbitrarily small experimental error, since the prediction (4) has some theoretical uncertainties, e.g. due to higher order corrections and proton form factor effects. Finally, the current experimental sensitivity [6] is still well below the prediction (4),

$$D_{\text{exp}} = (-0.6 \pm 1.0) \cdot 10^{-3}. \quad (5)$$

However, efforts are underway to improve the sensitivity by nearly an order of magnitude [4].

## 2.2 MSSM

Let us now turn to the calculation of the  $D$  parameter in the MSSM. We have extended the analysis of ref.[1] by including all possible diagrams at one loop order. Four different types of diagrams can contribute to neutron decay:

- vertex correction at the  $W$ –quark vertex;
- vertex correction at the  $W$ –lepton vertex;
- vertex corrections where the exchanged  $W$  boson is replaced by a charged Higgs boson;
- box diagrams.

The corrections to the  $W$ –lepton vertex give a contribution to  $D$  that is suppressed by a factor  $\frac{m_e}{m_p} \simeq 5 \cdot 10^{-4}$ , so these diagrams can safely be neglected compared to the corrections to the  $W$ –quark vertex. The diagrams with Higgs boson exchange do not contribute at all to the  $D$ –parameter, since they do not contain sufficiently many  $\gamma$  matrices to give rise to a spin correlation. We therefore only need to consider corrections to the  $W$ –quark vertex as well as box diagrams.

Since we are computing a contribution to the neutron decay distribution which has nontrivial dependence on final state momenta, see eq.(2), we cannot completely neglect external momenta when evaluating the loop integrals, even though these momenta are much smaller than the masses of the superparticles in the loop. However, after introducing Feynman parameters and shifting the loop integration variable  $k$  in such a way that the terms linear in

$k$  are eliminated from the denominator, all terms of order  $m_n$  or  $m_e$  can be neglected in the denominator; in other words, external momenta can be ignored in the loop integrals *after* the shift of the loop momentum. The three- and four-point functions that appear in our calculation can therefore easily be reduced to combinations of two-point functions, as described in Appendix C.

The coefficients in front of the loop integrals contain three different kinds of suppression factors. The Dirac algebra can introduce factors of the nucleon mass, rather than the mass of a fermionic superparticle. Moreover, certain chargino and neutralino couplings contain Yukawa couplings to first generation fermions. Finally, a term may require mixing between  $SU(2)$  doublet and singlet first generation sfermions, which is again proportional to a first generation Yukawa coupling. Numerically these three suppression factors are of comparable size, so that a simple counting of these factors is sufficient to isolate the leading terms.

Let us illustrate these remarks by analyzing the  $\tilde{\kappa}^0 - \tilde{u} - \tilde{d}$  loop correction to the  $Wud$  vertex, see Fig. 10 in Appendix B. The corresponding contribution to the  $D$  parameter is given in eq.(B.5). We first note that the three-point function  $C_{\mu\nu}$  is  $\mathcal{O}(1)$ , whereas the functions  $C_0$ ,  $C_{D2}$  and  $C_{D3}$ , which are defined in Appendix C, are  $\mathcal{O}(1/m_{\text{SUSY}}^2)$ , where  $m_{\text{SUSY}} \sim 0.1$  to 1 TeV is a typical superparticle mass scale. Let  $r \equiv m_n/m_{\text{SUSY}}$ , and  $Y_u$  and  $Y_d$  be the  $u$  and  $d$  quark Yukawa couplings, respectively. From eqs.(B.6) for the relevant couplings one can then derive the following behavior for the various terms listed in eq.(B.5), which we label here by the relevant product of couplings:

$$A_1 D_1 E_1 \sim \mathcal{O}(Y_u Y_d); \quad A_1 C_1 E_1 \sim \mathcal{O}(r Y_u); \quad B_1 D_1 E_1 \sim \mathcal{O}(r Y_d); \quad B_1 C_1 E_1 \sim \mathcal{O}(r^2). \quad (6)$$

We note that each term has two suppression factors. This is true for all other loop corrections as well, as can be seen from the results given in Appendix B. Terms with an even larger number of suppression factors have been omitted.

It should be noted that the terms containing powers of the suppression factor  $r$  have been obtained by replacing the kinematic  $u$  and  $d$  quark mass by the mass of the proton and neutron, respectively; this simple approximation goes under the name of “naive dimensional analysis” [7]. It seems reasonable to take some sort of long-distance quark mass here, although the use of a constituent quark mass  $\sim m_n/3$  could also be defended. Since the first generation Yukawa couplings are\*  $\mathcal{O}(10^{-4})$  one might think that  $Y_{u,d}$  give a much more severe suppression than  $r$ . However, this need not be the case. Only the imaginary parts of the products of couplings are relevant. Terms with explicit factors of Yukawa couplings can acquire nontrivial phases either from gaugino–higgsino mixing in the chargino–neutralino sector, or from mixing between  $SU(2)$  doublet and singlet sfermions, whereas (in the absence of sflavor mixing) terms without Yukawa couplings are generally not sensitive to phases in the sfermion sector. Note also that  $Y_d \propto \tan \beta$  for  $\tan \beta \gg 1$ . These considerations imply that contributions that are suppressed by Yukawa couplings are in general not smaller than those that are suppressed by powers of  $r$ . Finally, the box diagrams receive an additional (modest) suppression factor of order  $(m_W/m_{\text{SUSY}})^2$ . The same factor should also be multiplied to all terms that do not contain factors of  $r$ , while terms with only one power of  $r$  receive additional suppression of order  $m_W/m_{\text{SUSY}}$ . The reason is that heavy superparticles must decouple quadratically. Such factors result from mixing in the  $\tilde{\kappa}$  sector, and/or from mixing between  $SU(2)$  doublet and singlet squarks. [The latter is also suppressed by the relevant Yukawa coupling, but this is already included in eq.(6).] However, for reasonable superparticle masses these additional suppression factors are much less important than the factors listed in eq.(6).

---

\*These are short-distance couplings, to be taken at a momentum scale of order  $m_{\text{SUSY}}$ .

## 2.3 Restrictions on the parameter space

In order to make a useful analysis of the  $D$  parameter it is important to know which parts of the parameter space of the MSSM are still experimentally allowed. Especially relevant are experiments which test  $T$  symmetry violation in other observables, in particular the electric dipole moments (EDMs) of electron and neutron,  $d_e$  and  $d_n$ . Current experimental bounds on these quantities [6] impose strong constraints on parameter space. For superparticle masses of order (a few) hundred GeV, many combinations of phases are excluded, although in some cases there is a possibility that one can have small EDMs while retaining large phases [8]. For our analysis we have used the formulae for the EDMs given in [8], and checked for each parameter point that it does not violate the experimental limits

$$\begin{aligned} |d_n| &\leq 0.63 \cdot 10^{-25} \text{ e cm} & (\text{CL}=90\%) \\ -0.005 \cdot 10^{-26} \text{ e cm} &\leq d_e \leq 0.143 \cdot 10^{-26} \text{ e cm} & (\text{CL}=68\%) \end{aligned} \quad (7)$$

Of course, limits on superparticle masses from null results of experimental searches for these particles at high energy colliders also have to be respected [6].

## 3 Numerical Analysis

### 3.1 Choice of Parameters

We wish to find the maximal supersymmetric contribution to  $D$  in the framework of the  $R$ –parity conserving MSSM. As well known, the parameter space of the general MSSM is vast, so some simplifying assumptions are necessary. In our analysis we have assumed that no flavor mixing exists in the sfermion sector. This means that the  $f\tilde{f}\tilde{\kappa}^0$  and  $f\tilde{f}\tilde{g}$  vertices are diagonal in flavor space. One can then easily see from the diagrams given in Appendix B that CKM mixing between quarks is not relevant, i.e. all sfermions in the loop must be of the first generation. On the other hand, our discussion of eq.(6) showed that it is of crucial importance to include  $L - R$  mixing even for first generation squarks.

Ignoring all flavor mixing between sfermions may sound like a rather severe restriction on the parameter space. However, mixing between first generation sfermions and those of the second or third generation is strongly constrained by experimental limits on various FCNC processes [9]. We have checked that including flavor off-diagonal  $LR$  and  $RL$  entries of the experimentally allowed magnitude in the squark mass matrices does not increase the maximal contribution to  $D$  once the constraints (7) on the EDMs have been imposed. Generally speaking, flavor mixing should not be very important here, since all external fermions belong to the same (first) generation.

In the absence of flavor mixing between sfermions our results are independent of the soft breaking parameters describing the second and third generation sfermion mass matrices. The same is true for the soft breaking parameters of the tree-level Higgs potential. We have initially chosen a rather small value for the ratio of vacuum expectation values (vevs)  $\tan\beta$ ,

$$\tan\beta = 3. \quad (8)$$

The reason is that supersymmetric contributions to the EDMs increase with  $\tan\beta$  [8]. Choosing a small value for this parameter therefore minimizes the impact of the experimental constraints (7) on the allowed values of the remaining parameters.

Supersymmetry is a decoupling theory, which means that in the limit where the masses of the supersymmetric particles go to infinity, the predictions for all observables approach their SM values. We therefore consider a relatively light spectrum of superparticles, described by the following values of the relevant soft breaking parameters:

$$m_L^2 = 35 \cdot 10^3 \text{ GeV}^2 \quad m_R^2 = 50 \cdot 10^3 \text{ GeV}^2 \quad (9a)$$

$$m_Q^2 = 150 \cdot 10^3 \text{ GeV}^2 \quad m_U^2 = m_D^2 = 200 \cdot 10^3 \text{ GeV}^2 \quad (9b)$$

$$|\mu| = 450 \text{ GeV} \quad (9c)$$

$$|m_1| = 200 \text{ GeV} \quad |m_2| = 400 \text{ GeV} \quad |m_3| = 800 \text{ GeV} \quad (9d)$$

Here  $m_L$  and  $m_R$  are the soft breaking masses for  $SU(2)$  doublet and singlet sleptons,  $m_Q$  is the soft breaking mass for  $SU(2)$  doublet squarks, and  $m_U$  and  $m_D$  are the soft breaking masses for  $SU(2)$  singlet squarks with charge  $2/3$  and  $-1/3$ , respectively; recall that we only need to specify these masses for the first generation. As mentioned earlier,  $\mu$  is the coefficient of the term coupling the two Higgs superfields in the superpotential. Finally,  $m_i$  are the soft breaking gaugino masses; the ratios of these masses are similar to that expected in Grand Unified models with universal gaugino mass at the unification scale. The choices (9) lead to a superparticle spectrum that respects all experimental limits from searches for superparticles, and allows large CP-violating phases through the cancellation mechanism [8]. We will later comment on the effect of lowering the overall SUSY mass scale from the choice of eqs.(9).

The remaining parameters are sampled randomly, taking a flat distribution within specified limits. The trilinear couplings<sup>†</sup>

$$|A_u| \equiv |A_d|, |A_l| \in [0, 0.1] \text{ GeV} \quad (10)$$

were chosen so that internal cancellations in the EDMs are possible but the sfermions do not acquire vevs, which would be the case for too large values. For simplicity we took the same value for  $A_d$  and  $A_u$ ;  $A_l$  is allowed to differ, in order to facilitate independent cancellations in the supersymmetric contributions to  $d_n$  and  $d_e$ . Finally the phases of the gaugino masses,  $\mu$  and of the trilinear couplings were varied independently (except  $A_d \equiv A_u$ ) over the entire possible range,

$$\phi_{m_1}, \phi_{m_2}, \phi_{A_u} \equiv \phi_{A_d}, \phi_{A_l}, \phi_\mu \in [0, 2\pi[. \quad (11)$$

Note that by an appropriate field redefinition the phase of the gluino mass can always be set to zero without loss of generality.

## 3.2 Numerical Results

In this section we display the results of our numerical analysis. Note that only about 20,000 out of  $10^{10}$  tested sets of parameters satisfied the constraints (7). This illustrates that the EDMs do indeed severely constrain the allowed combinations of nontrivial complex phases in the MSSM Lagrangian.

In Fig. 1 we plot the dependence of the supersymmetric contribution  $D_{\text{SUSY}}$  to the  $D$  parameter on the phase  $\phi_\mu$ . It is easy to see that  $D_{\text{SUSY}}$  depends strongly on this phase. There is however also a large variability at fixed  $\phi_\mu$ , which shows that  $D_{\text{SUSY}}$  also depends significantly on the other parameters.

---

<sup>†</sup>Recall that we are using the convention of ref.[2], where the ordinary Yukawa couplings are explicitly included in the  $A$ -parameters. In case of first generation quarks these couplings are roughly of order  $10^{-4}$ ; this explains the small values of the  $A$ -parameters in eq.(10).

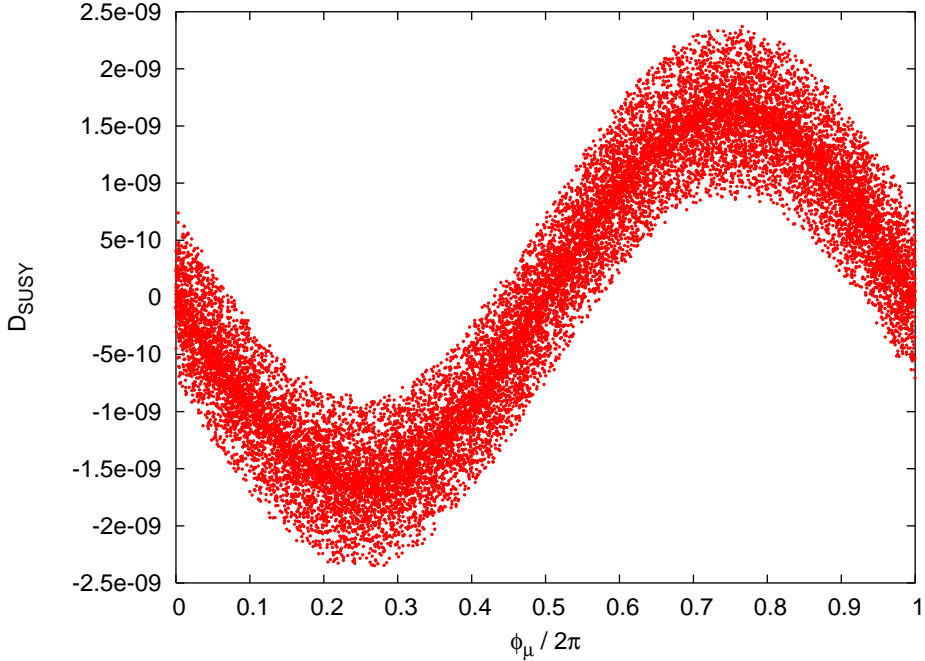


Figure 1: Supersymmetric contribution to the  $D$  parameter depending on the phase  $\phi_\mu$ .

Before investigating this closer it is useful to identify the diagram which gives the leading supersymmetric contribution to  $D$ . Inspection of the contributing diagrams in Appendix B shows that only one of them, the quark vertex correction shown in Fig. 11, involves the strong interactions. One might have thought that the presence of the gluino in this diagram, which is significantly heavier than the electroweak gauginos, would partially compensate this enhancement. However, this would only be true if the gluino was significantly heavier than the squarks in the loop; such an ordering of masses is not allowed in the MSSM, since it would lead to tachyonic squark masses at energy scales just above the gluino mass [10]. Indeed we find numerically that the gluino vertex diagram, which is the only diagram considered in [1], gives the leading contribution to  $D_{\text{SUSY}}$ . All other diagrams are suppressed by at least one order of magnitude. This is in spite of the fact that the only phases contributing to the gluino loop diagram come from squark mixing, whereas the electroweak loop corrections are also sensitive to phases from electroweak gaugino–higgsino mixing.<sup>‡</sup> On the other hand, the relative importance of the other diagrams is increased by the fact that they *all* add destructively to the gluino loop diagram, i.e. tend to reduce  $|D_{\text{SUSY}}|$ . As a result, the pure gluino loop contribution to  $D_{\text{SUSY}}$ , shown in Fig. 2, is somewhat larger in absolute size than the total one-loop contribution shown in Fig. 1.

The contributions of the other five diagrams are shown in Fig. 3. For better readability the  $y$ –axis was scaled down by a factor of 10. The numbers in brackets in the label of the  $y$  axis denote the diagram whose contribution is shown in the corresponding plot.

We see that the first of the three electroweak vertex corrections, with a neutralino and two squarks in the loop, gives significantly larger contributions than diagrams 3 and 4, which have one squark, one chargino and one neutralino in the loop. This can be understood from the

<sup>‡</sup>Partly for this reason, the chargino and gluino loop contributions to  $d_n$  can be of similar size. Note, however, that in case of the  $D$  parameter the chargino and gluino loop contributions have quite different structure, i.e. there is no chargino diagram with two squark propagators.

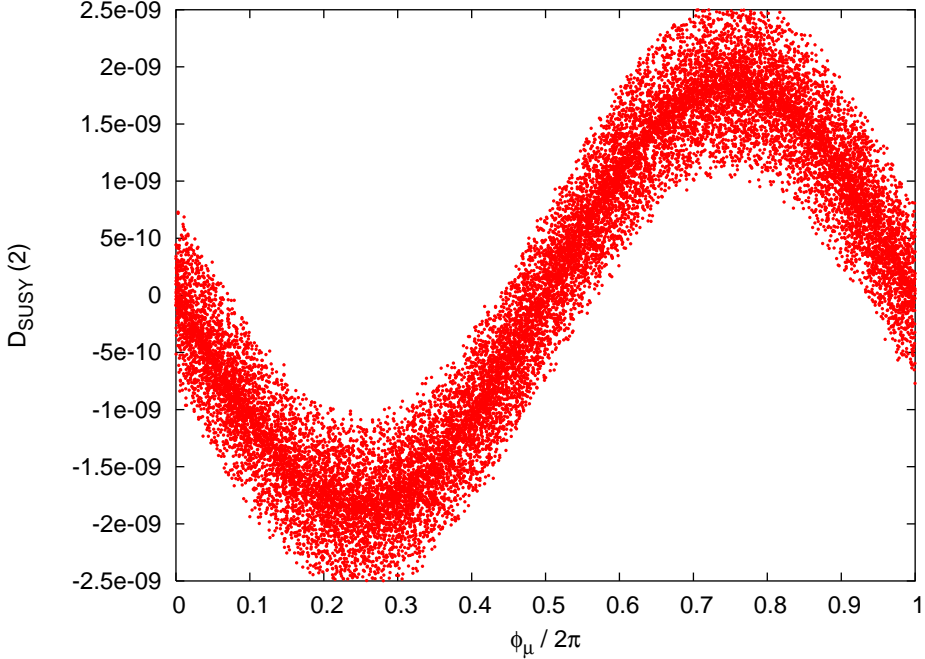


Figure 2: The contribution from the leading gluino diagram to  $D_{\text{SUSY}}$ .

observation that the  $W\tilde{\kappa}_i^\pm\tilde{\kappa}_j^0$  vertex only couples two  $SU(2)$  gauginos (winos) or two higgsinos together; this suppresses possible contributions involving the phase  $\phi_1$  associated with the  $U(1)_Y$  gaugino (bino). Moreover, the coupling structure in diagrams 3 and 4 is such that some gaugino–higgsino mixing is required, whereas diagram 1 gets finite contributions even without this mixing. This suppresses the contributions of diagrams 3 and 4 by a factor  $\mathcal{O}(m_W/m_{\text{SUSY}})$  relative to that of diagram 1. Finally, for the given choice of sparticle masses, the box diagrams 5 and 6 give contributions which are about two orders of magnitude smaller than that of diagrams 3 and 4. We remarked earlier that the contribution from box diagrams are suppressed by  $(m_W/m_{\text{SUSY}})^2 \simeq 1/20$  for our set of parameters. Moreover, the additional integration over Feynman parameters required in the  $D$ –functions appearing in the box contributions gives another suppression factor  $\sim 1/5$  compared to the  $C$ –functions appearing in the vertex corrections.

Let us now return to the question which other parameters influence the size of  $D_{\text{SUSY}}$ . As the gluino diagram is independent of the phases  $\phi_{m_1}$  and  $\phi_{m_2}$  these cannot play significant roles. If we now restrict  $\phi_\mu$  to a small interval around  $\pi$  ( $\phi_\mu = \pi \pm 0.01\pi$ ), in accordance with the limits on the EDMs, it becomes clear that  $A_u$  is the second parameter which determines  $D_{\text{SUSY}}$  for given sparticle masses.  $|A_u|$  largely determines the amount of  $L-R$  mixing between up-type squarks, since in this case the contribution  $\propto |\mu|$  is suppressed by a factor  $\cot\beta$ ; many of the terms  $\propto Y_u$  originate from this mixing. Since  $\mu$  is almost real,  $|D_{\text{SUSY}}|$  becomes very small as  $|A_u| \rightarrow 0$ , as shown in Fig. 4. Moreover, for (almost) real  $\mu$ , the phase of  $A_u$  ( $= A_d$  for our choice of parameters) determines the CP–violating phases in the squark mixing matrices. This leads us to expect that  $|D_{\text{SUSY}}|$  will be maximal if  $\phi_{A_u}$  is  $\sim \frac{\pi}{2}$  or  $\sim \frac{3\pi}{2}$ . This is confirmed by Fig. 5. ( $|D_{\text{SUSY}}|$  can be small even for these choices of  $\phi_{A_u}$  since  $|A_u|$  is still varied in Fig. 5; of course, the value of  $\phi_{A_u}$  becomes irrelevant as  $|A_u| \rightarrow 0$ .)

We have also investigated the influence of  $\tan\beta$  on  $D_{\text{SUSY}}$ . To that end the parameter

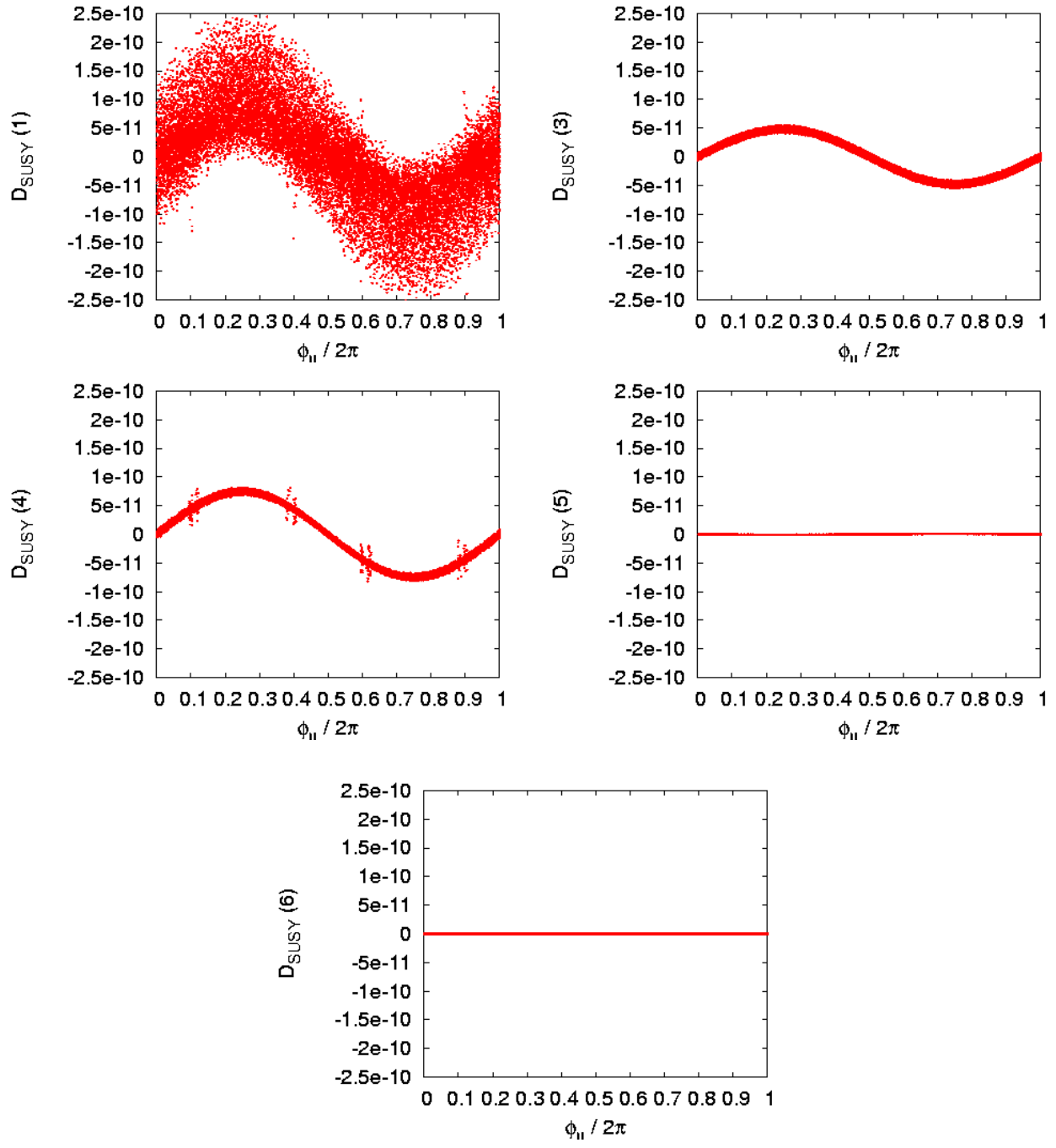


Figure 3: Electroweak contributions to  $D_{\text{SUSY}}$ . The numbers in parentheses correspond to the labeling of diagrams and their contributions in Appendix B; e.g.  $D_{\text{SUSY}}(1)$  refers to the diagram shown in Fig. 10, whose contribution is given by eq.(B.5).

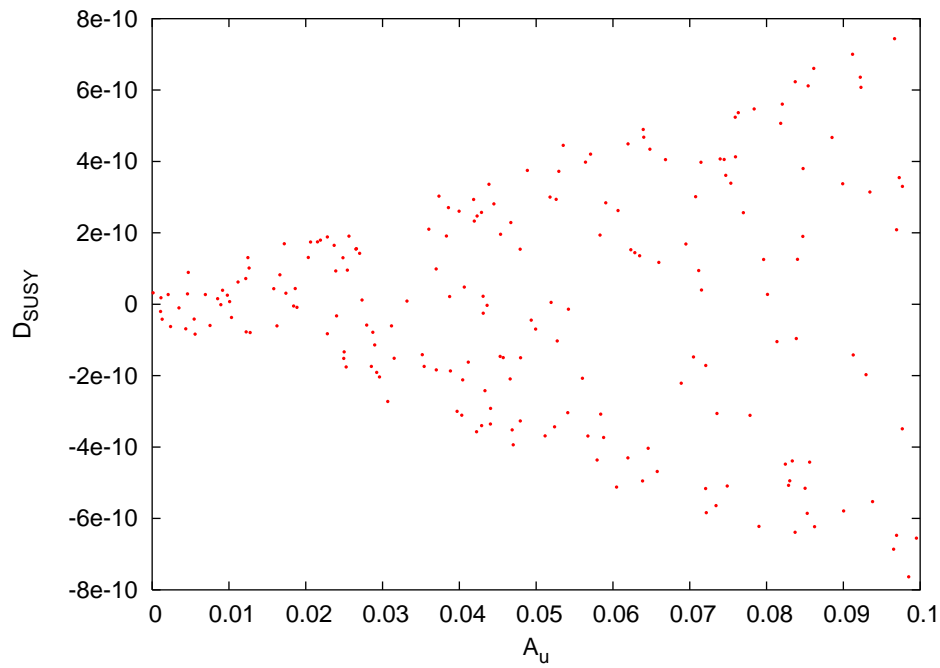


Figure 4:  $D_{\text{SUSY}}$  vs.  $A_u$  at  $\phi_\mu \approx \pi$

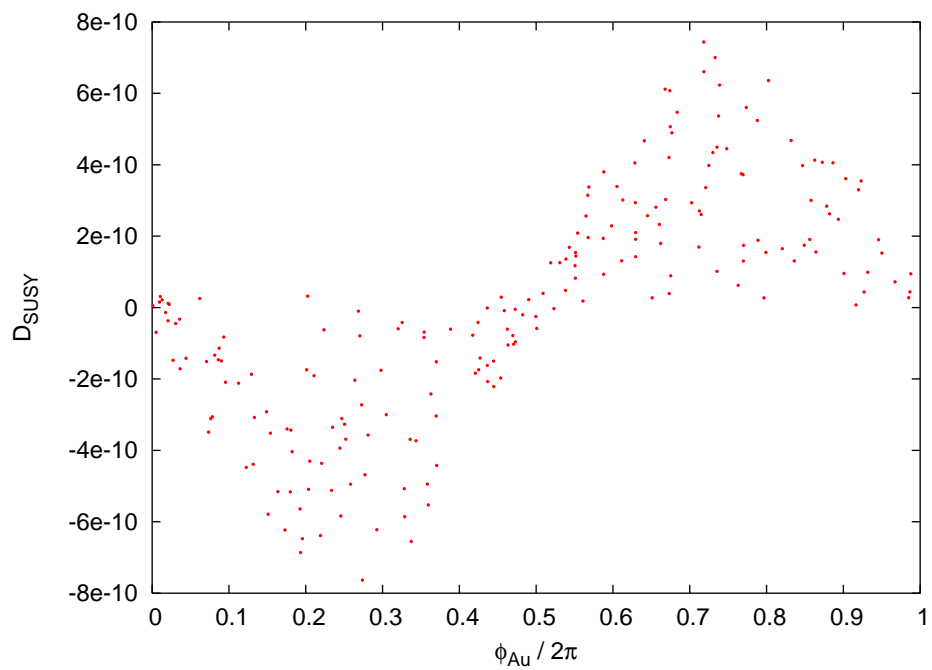


Figure 5:  $D_{\text{SUSY}}$  vs.  $\phi_{A_u}$  at  $\phi_\mu \approx \pi$

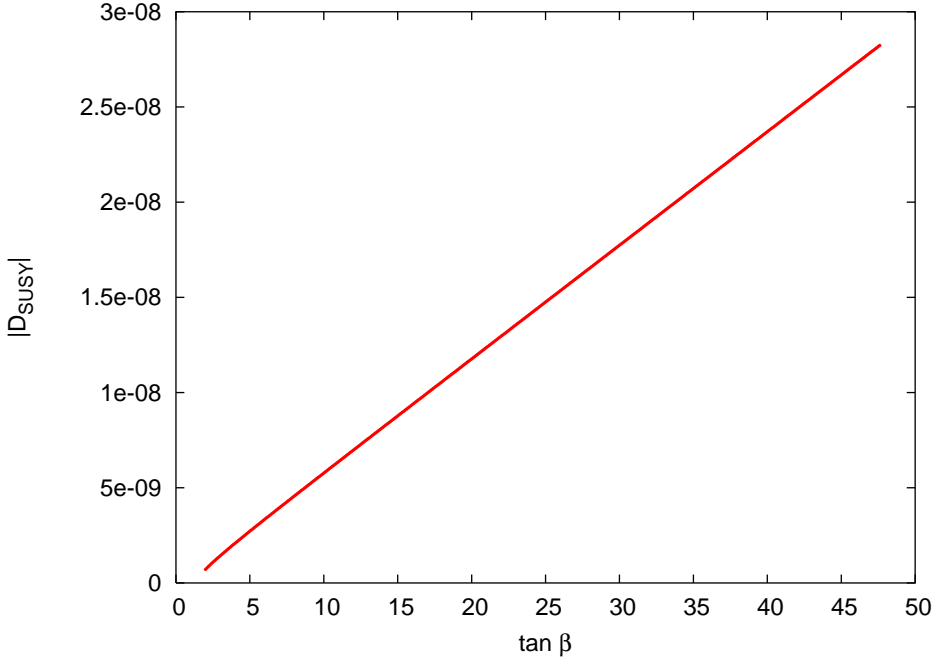


Figure 6:  $D_{\text{SUSY}}$  as function of  $\tan \beta$ , for the parameter set (12).

point

$$\begin{aligned}
 \phi_{m_2} &= 0.8135\pi & \phi_{m_1} &= 0.09748\pi & \phi_\mu &= 1.4175\pi \\
 |A_u| &= 0.02279 \text{ GeV} & \phi_{A_u} &= 0.2972\pi
 \end{aligned} \tag{12}$$

was chosen arbitrarily from the set of points that are allowed for  $\tan \beta = 3$ . The  $\tan \beta$  dependence of  $D_{\text{SUSY}}$  is shown in Fig. 6. The almost linear increase results from the increase of the  $d$ -quark Yukawa coupling, and hence of  $\tilde{d}_L - \tilde{d}_R$  mixing, which is proportional to  $1/\cos \beta \simeq \tan \beta$  for  $\tan^2 \beta \gg 1$ . Here we have neglected the restrictions from the EDMs; for the set of parameters described by eqs.(9), (10) and (12), these impose the bound  $\tan \beta < 3.5$ . On the other hand, since several contributions to  $d_e$  and  $d_n$  grow  $\propto \tan \beta$ , cancellations can also work at large  $\tan \beta$ , if some of the other parameters, e.g. the phases, are changed slightly, without significantly modifying the prediction for  $D_{\text{SUSY}}$ . However, since the separate contributions to  $d_e$  and  $d_n$  grow with increasing  $\tan \beta$ , increasingly precise cancellations become necessary to satisfy the experimental constraints (7).

Both of these observations are confirmed by Fig. 7, which shows  $D_{\text{SUSY}}$  for the same parameters as in Fig. 1, except that now  $\tan \beta = 30$ . We see that the overall scale of  $D_{\text{SUSY}}$  is one order of magnitude larger than in Fig. 1, as expected from the linear growth shown in Fig. 6. The small number of surviving points illustrates the difficulty of getting both  $|d_e|$  and  $|d_n|$  sufficiently small through delicate cancellations. In particular, the  $d_e$  constraint now excludes some region of  $\phi_\mu$  altogether.<sup>§</sup> Recall, however, that the (s)leptonic corrections to  $D_{\text{SUSY}}$  are suppressed by a factor  $m_e/m_p$ , and are thus negligible. We can therefore vary the sleptonic soft breaking masses  $m_L, m_R$  without significantly changing the prediction for  $D_{\text{SUSY}}$ . In this case the entire range of  $\phi_\mu$  becomes allowed again. We therefore conclude that

<sup>§</sup>Recall that  $\phi_\mu$  measures the relative phase between  $\mu$  and the gluino mass  $m_3$ . For the choice (9) of dimensional parameters the  $d_e$  constraint limits the relative phase between  $\mu$  and the  $SU(2)$  gaugino mass  $m_2$  to narrow bands around 0 and  $\pi$  even for small  $\tan \beta$ , but this is not visible after scanning over  $\phi_{m_2}$ .

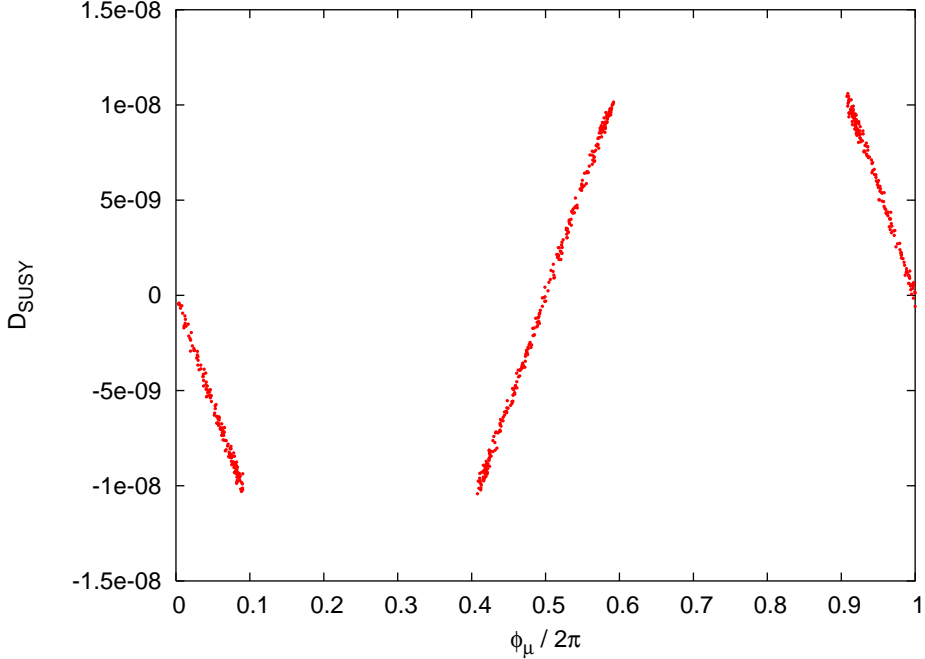


Figure 7:  $D_{\text{SUSY}}$  vs.  $\phi_\mu$  for  $\tan \beta = 30$ .

the maximal allowed  $|D_{\text{SUSY}}|$  increases essentially linearly with  $\tan \beta$ . However, requiring the bottom Yukawa coupling to be less than that of the top quark, or at least to be sufficiently small to not have a Landau pole below the scale of Grand Unification, leads to the upper bound  $\tan \beta \lesssim 60$ . If the dimensionful parameters in the squark, gaugino and higgsino sectors are as in eqs.(9), the maximal value of  $|D_{\text{SUSY}}|$  is therefore around  $5 \cdot 10^{-8}$ .

Our choice (9) for the relevant soft breaking masses means that first generation squarks as well as most charginos and neutralinos have masses around 400 to 500 GeV. Direct searches for sparticles allow us to lower these masses by a factor of two to three. We expect that for fixed phases  $D$  scales quadratically with the overall superparticle mass scale,  $D \propto 1/m_{\text{SUSY}}^2$ .

This is borne out by Fig. 8, which shows  $D_{\text{SUSY}}$  for  $\tan \beta = 3$ ; the other parameters are as in eqs.(9) and (12), except that all quantities with mass dimension are multiplied with the dimensionless factor  $c$ , which is varied between 0.4 and 2. Similar to the case of Fig. 6, values of  $c$  significantly different from unity are disallowed by the constraints on  $d_e$  and/or  $d_n$ , but again this can be fixed by small variations of the phases. Since  $D_{\text{SUSY}}$  and the dipole moments show the same  $c^{-2}$  dependence on  $c$ , increasingly delicate cancellations are required to satisfy the constraints (7) as  $c$  is reduced. The lower bound  $c \geq 0.44$  is in our case set by the lower bound on the mass of the lightest selectron,  $m_{\tilde{e}} \geq 95$  GeV, from LEP searches [6].

By simultaneously reducing the overall SUSY mass scale *and* increasing  $\tan \beta$  one might therefore in principle be able to reach values of  $|D_{\text{SUSY}}|$  slightly above  $10^{-7}$ . However, the finetuning required to satisfy the limits on both  $d_e$  and  $d_n$  then becomes very severe indeed; less than one parameter set in  $10^9$  will survive.<sup>¶</sup> Moreover, one would have to choose soft breaking masses for  $\tilde{\tau}$  sleptons and  $\tilde{b}$  squarks that are much larger than those for the corresponding first generation sfermions. Otherwise  $L - R$  mixing, which grows  $\propto |\mu| \tan \beta$ , would make the lighter  $\tilde{\tau}$  and  $\tilde{b}$  mass eigenstates much too light, or even tachyonic. Recall that even  $|D_{\text{SUSY}}| \simeq 10^{-7}$  is still two orders of magnitude below the contribution (4) from final state

<sup>¶</sup>Since  $d_e$  and  $d_n$  have to be finetuned independently, the overall severity of finetuning scales like  $c^{-4} \cdot \tan^2 \beta$ .

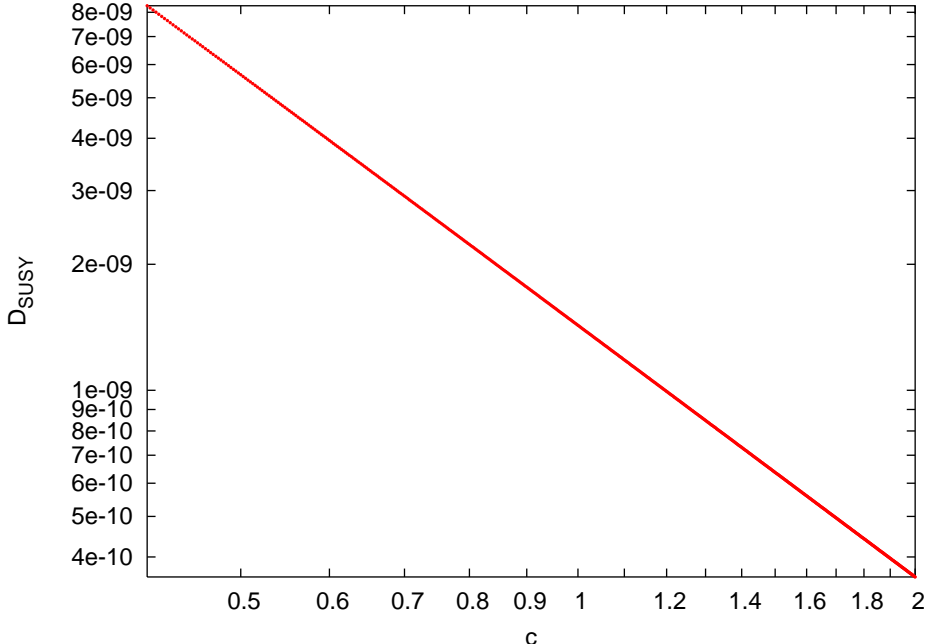


Figure 8:  $D_{SUSY}$  for  $\tan \beta = 3$ , where the other parameters are as in eqs.(9) and (12), except that all mass parameters have been multiplied with the dimensionless scaling factor  $c$ .

interactions.

Finally, we have checked for a few cases that changing the ratios of soft breaking parameters from the choice of eqs.(9) does not increase the maximal allowed value of  $D_{SUSY}$  significantly. This is not surprising, since the overall scale of  $D_{SUSY}$  is set by the *heaviest* superparticle that occurs in a given loop diagram, whereas the lower bound on the overall mass scale is essentially set by the *lightest* (charged) superparticle.  $|D_{SUSY}|$  will therefore be maximal if the parameters are chosen such that the mass splitting between superparticles is relatively small, which is true for the parameters of eqs.(9).

## 4 Conclusions and Outlook

In this paper we have analyzed  $T$  symmetry violation in the beta decay of free neutrons via the  $D$  parameter. We have extended the analysis of [1] by computing all diagrams that occur at one loop order. We have performed a full scan of the allowed phases and the magnitude of the  $A$  parameters describing mixing between  $SU(2)$  singlet and doublet squarks, subject only to the experimental constraints on the electric dipole moments of the electron and, in particular, the neutron.

We find that the gluino loop correction to the  $Wud$  vertex indeed gives the leading supersymmetric contribution to  $D$ . The phase of  $\mu$ , which has been neglected in ref.[1], crucially influences the size of  $D_{SUSY}$ . Moreover, allowing for cancellations between various contributions to the EDMs permits larger values for the relevant phases, which increases  $|D_{SUSY}|$ . We nevertheless find that the maximal contribution to  $|D|$  from the  $R$ –parity conserving MSSM is at least two orders of magnitude smaller than the contribution (4) from electromagnetic final state interactions. This means that even greatly improved experimental upper bounds on  $|D|$  will not lead to new constraints on this model. On the other hand, a measurement of  $D$  which

differs significantly from the prediction (4) would rule out the  $R$ –parity conserving MSSM along with the SM. Larger contributions might be possible in the  $R$ –parity violating version of the MSSM. Note that  $R$ –parity violation only through trilinear terms in the superpotential does not contribute to the EDMs at one–loop level [11], whereas e.g. baryon–number violating ( $\lambda''$ ) couplings can contribute to  $D$  at the one–loop level.

Analogous triple products can also be defined for decays involving heavier particles than the neutron. Decays of heavier baryons, e.g.  $\Lambda$  or  $\Lambda_b$ , can be treated using the expressions given in Appendix B, since here the external momenta are still much smaller than  $m_{\text{SUSY}}$ . In these cases the supersymmetric contributions are expected to be larger by several orders of magnitude than in case of neutron decay, since  $Y_d$  would be replaced by  $Y_s$  or even  $Y_b$ ; in addition, the constraints on CP–violating phases of soft breaking parameters in the second and third generation are much weaker than for the first generation. Experimental measurements will probably be difficult in these cases, however.

Even larger supersymmetric contributions can be expected for the analogous asymmetry in top quark decay. Since the top Yukawa coupling is  $\mathcal{O}(1)$ , electroweak corrections might well be comparable to SUSY QCD corrections [1] in this case. Moreover, the mass ratio  $m_t/m_{\text{SUSY}}$  is also  $\mathcal{O}(1)$ . This again increases the level of the expected corrections; it also means, however, that the expansion for small external momenta used in our calculation is no longer adequate. Note also that the spin of the top quark cannot be measured directly; nevertheless the  $D$ –parameter in top decays does contribute to measurable  $T$ –odd asymmetries [12]. The final state interactions for such decays have already been found to have approximately the same size as for neutron decay [13]. A full calculation of supersymmetric contributions to CP–violation in top decay, including electroweak contributions, might therefore prove rewarding.

## Acknowledgements

We thank Janusz Rosiek for providing us with FORTRAN code for the diagonalization of the mass matrices and for the evaluation of some loop functions, and Athanasios Dedes for useful discussions. This work was partially supported by the SFB 375 of the Deutsche Forschungsgemeinschaft.

## A Notation

For the benefit of the reader we have summarized in this appendix the conventions used in this paper. A complete description including all expressions for the Feynman rules can be found in [2].

There are two charginos  $\kappa_i^\pm, i = 1, 2$  whose mass matrix is diagonalized by two unitary matrices  $Z_+$  and  $Z_-$ :

$$(Z_-)^T \begin{pmatrix} m_2 & \frac{ev_2}{\sqrt{2}s_W} \\ \frac{ev_1}{\sqrt{2}s_W} & \mu \end{pmatrix} Z_+ = \text{diag}(m_{\kappa_1^\pm}, m_{\kappa_2^\pm}) \quad (\text{A.1})$$

This equation does not specify the two matrices  $Z_+$  and  $Z_-$  uniquely. This can be used to choose both masses positive and sorted in ascending order.

Similarly, the neutralinos are denoted by  $\kappa_i^0, i = 1 \dots 4$  and the neutralino mass matrix is

diagonalized by a unitary matrix  $Z_N$  such that

$$(Z_N)^T \begin{pmatrix} m_1 & 0 & \frac{-ev_1}{2c_W} & \frac{ev_2}{2c_W} \\ 0 & m_2 & \frac{ev_1}{2s_W} & \frac{-ev_2}{2s_W} \\ \frac{-ev_1}{2c_W} & \frac{ev_1}{2s_W} & 0 & -\mu \\ \frac{ev_2}{2c_W} & \frac{-ev_2}{2s_W} & -\mu & 0 \end{pmatrix} Z_N = \text{diag}(m_{\kappa_1^0}, \dots, m_{\kappa_4^0}) \quad (\text{A.2})$$

As noted in the text, the mass parameter of the  $SU(3)$  gauginos can be taken as real. Therefore the eight gluinos all have a mass of  $m_3$ .

Finally, the sfermion mass matrix can be written compactly for all four different types of sfermions as

$$\mathcal{M}_{\tilde{f}}^2 = \begin{pmatrix} m_{\tilde{f}_L}^2 + m_f^2 + \frac{e^2(v_1^2 - v_2^2)(T_f^3 - Q_f s_W^2)}{4s_W^2 c_W^2} & -m_f \left( \kappa \mu^* + \frac{A_f}{Y} \right) \\ -m_f \left( \kappa \mu + \frac{A_f^*}{Y} \right) & m_{\tilde{f}_R}^2 + m_f^2 + Q_f \frac{e^2(v_1^2 - v_2^2)}{4c_W^2} \end{pmatrix} \quad (\text{A.3})$$

Here,  $\kappa = \cot \beta$  for up-type squarks and  $\kappa = \tan \beta$  for down-type squarks and charged sleptons.  $m_{\tilde{f}_L}$  and  $m_{\tilde{f}_R}$  denote the mass parameters and  $A_f$  the coefficient of the trilinear terms from the soft SUSY-breaking terms in the Lagrangian, and  $Y$  is the respective Yukawa coupling.  $Q_f$  is the electromagnetic charge and  $T_f^3$  the quantum number of the third component of the isospin operator. As there is no  $SU(2)$  singlet sneutrino only the upper left element in the matrix of eq. A.3 occurs for the sneutrinos.

These mass matrices can be diagonalized with a unitary matrix each, yielding

$$\begin{aligned} Z_\nu^T \mathcal{M}_{\tilde{\nu}}^2 Z_\nu^* &= \text{diag}(m_{\tilde{\nu}_1}^2, \dots, m_{\tilde{\nu}_3}^2) & Z_L^\dagger \mathcal{M}_{\tilde{e}}^2 Z_L &= \text{diag}(m_{\tilde{e}_1}^2, \dots, m_{\tilde{e}_6}^2) \\ Z_U^T \mathcal{M}_{\tilde{u}}^2 Z_U^* &= \text{diag}(m_{\tilde{u}_1}^2, \dots, m_{\tilde{u}_6}^2) & Z_D^\dagger \mathcal{M}_{\tilde{d}}^2 Z_D &= \text{diag}(m_{\tilde{d}_1}^2, \dots, m_{\tilde{d}_6}^2) \end{aligned} \quad (\text{A.4})$$

## B Feynman diagrams

Altogether six Feynman diagrams were computed. The vertex corrections at the W-lepton vertex are, as already mentioned, suppressed by a factor of  $\frac{m_e}{m_p} \simeq 5 \cdot 10^{-4}$  and can therefore be neglected. We first give the tree level expression for the differential decay distribution, since it enters the definition of the  $D$ -parameter:

$$D = \frac{d\Gamma_i}{dE_e d \cos \theta_{e\bar{\nu}}} / \left( \frac{d\Gamma_{\text{tree}}}{dE_e d \cos \theta_{e\bar{\nu}}} \cdot \vec{s}_n \cdot \left( \frac{\vec{p}_e \times \vec{p}_{\bar{\nu}}}{E_e E_{\bar{\nu}}} \right) \right) \quad (\text{B.1})$$

All necessary traces have been computed with the help of FORM [14]; in many cases the results have been checked using manual calculations.

### Tree level result

$$\frac{d\Gamma_{\text{tree}}}{dE_e d \cos \theta_{e\bar{\nu}}} = \frac{E_{\bar{\nu}}^2 \sqrt{E_e^2 - m_e^2}}{8\pi^3 m_W^4 (m_n - E_e - E_{\bar{\nu}})} E_e m_n U^2 V^2 \quad (\text{B.2})$$

with

$$U = -\frac{e}{\sqrt{2} \sin \theta_W} C^{IJ} \quad (\text{B.3})$$

$$V = -\frac{e}{\sqrt{2} \sin \theta_W} \delta^{KL}. \quad (\text{B.4})$$

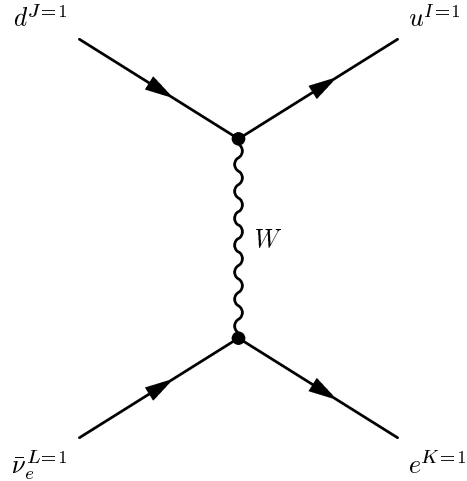


Figure 9: Tree level diagram describing neutron decay.

Here  $e$  is the QED coupling constant,  $\theta_W$  the weak mixing angle, and  $C$  the quark flavor mixing matrix. In our numerical calculation we have ignored all flavor mixing.

**Diagram 1: Neutralino- $\tilde{u}$ - $\tilde{d}$  vertex correction**

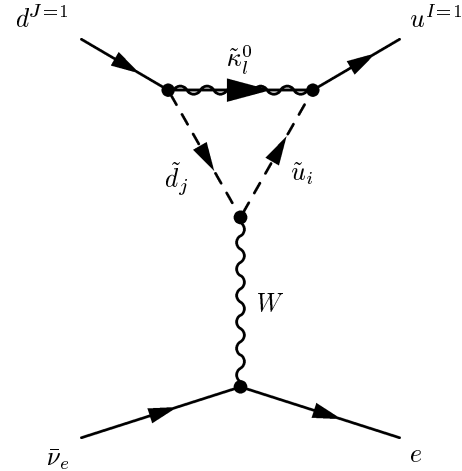


Figure 10: Vertex correction with neutralino- $\tilde{u}$ - $\tilde{d}$  loop.

$$\begin{aligned}
\frac{d\Gamma_1}{dE_e d \cos \theta_{e\bar{\nu}}} = & \frac{d\Gamma_{\text{tree}}}{dE_e d \cos \theta_{e\bar{\nu}}} \cdot \vec{s}_n \cdot \left( \frac{\vec{p}_e \times \vec{p}_{\bar{\nu}}}{E_e E_{\bar{\nu}}} \right) \frac{1}{4m_n U^2 V^2} \frac{\Re(UV^2)}{16\pi^2} \\
& \left[ \left( -2\Im(A_1 D_1 E_1) m_p \right) C_{\mu\nu}(0, 0, m_{\tilde{u}_i}, m_{\tilde{d}_j}, m_{\tilde{\kappa}_l^0}) \delta^{\mu\nu} \right. \\
& + \left( 4\Im(A_1 C_1 E_1) + 4\Im(B_1 D_1 E_1) \right) m_{\tilde{\kappa}_l^0} m_n^2 C_{D2}(0, 0, m_{\tilde{\kappa}_l^0}, m_{\tilde{u}_i}, m_{\tilde{d}_j}) \\
& + 4\Im(B_1 C_1 E_1) m_n^3 \left( C_{D2}(0, 0, m_{\tilde{\kappa}_l^0}, m_{\tilde{u}_i}, m_{\tilde{d}_j}) - C_{D3}(0, 0, m_{\tilde{\kappa}_l^0}, m_{\tilde{u}_i}, m_{\tilde{d}_j}) \right) \Big] \\
& + \dots
\end{aligned} \tag{B.5}$$

with

$$A_1 = \frac{2\sqrt{2}e}{3 \cos \theta_W} Z_U^{(I+3)i} Z_N^{1l} - Y_u^I Z_N^{4l} Z_U^{Ii} \tag{B.6a}$$

$$B_1 = - \frac{e}{\sqrt{2} \sin \theta_W \cos \theta_W} Z_U^{Ii} \left( \frac{1}{3} Z_N^{1l*} \sin \theta_W + Z_N^{2l*} \cos \theta_W \right) - Y_u^I Z_N^{4l*} Z_U^{(I+3)i} \tag{B.6b}$$

$$C_1 = - \frac{e}{\sqrt{2} \sin \theta_W \cos \theta_W} Z_D^{Jj} \left( \frac{1}{3} Z_N^{1l} \sin \theta_W - Z_N^{2l} \cos \theta_W \right) + Y_d^J Z_D^{(J+3)j} Z_N^{3l} \tag{B.6c}$$

$$D_1 = \frac{-\sqrt{2}e}{3 \cos \theta_W} Z_D^{(J+3)j} Z_N^{1l*} + Y_d^J Z_D^{Jj} Z_N^{3l*} \tag{B.6d}$$

$$E_1 = - \frac{e}{\sqrt{2} \sin \theta_W} Z_D^{Jj*} Z_U^{Ii*} C^{IJ} \tag{B.6e}$$

The dots (...) denote additional terms in the decay distribution that do not contribute to  $D$ . Eqs. (B.5) and (B.6), as well as all subsequent expressions, are given in the notation of Rosiek [2].

**Diagram 2: Gluino- $\tilde{u}$ - $\tilde{d}$  vertex correction.**

$$\begin{aligned}
\frac{d\Gamma_2}{dE_e d \cos \theta_{e\bar{\nu}}} = & \frac{d\Gamma_{\text{tree}}}{dE_e d \cos \theta_{e\bar{\nu}}} \cdot \vec{s}_n \cdot \left( \frac{\vec{p}_e \times \vec{p}_{\bar{\nu}}}{E_e E_{\bar{\nu}}} \right) \frac{4}{3} \frac{1}{4m_n U^2 V^2} \frac{\Re(UV^2)}{16\pi^2} \\
& \left[ \left( -2\Im(A_2 D_2 E_2) m_p \right) C_{\mu\nu}(0, 0, m_{\tilde{u}_i}, m_{\tilde{d}_j}, m_{\tilde{g}_l}) \delta^{\mu\nu} \right. \\
& + \left( 4\Im(A_2 C_2 E_2) + 4\Im(B_2 D_2 E_2) \right) m_{\tilde{g}_l} m_n^2 C_{D2}(0, 0, m_{\tilde{g}_l}, m_{\tilde{u}_i}, m_{\tilde{d}_j}) \\
& + 4\Im(B_2 C_2 E_2) m_n^3 \left( C_{D2}(0, 0, m_{\tilde{g}_l}, m_{\tilde{u}_i}, m_{\tilde{d}_j}) - C_{D3}(0, 0, m_{\tilde{g}_l}, m_{\tilde{u}_i}, m_{\tilde{d}_j}) \right) \Big] \\
& + \dots
\end{aligned} \tag{B.7}$$

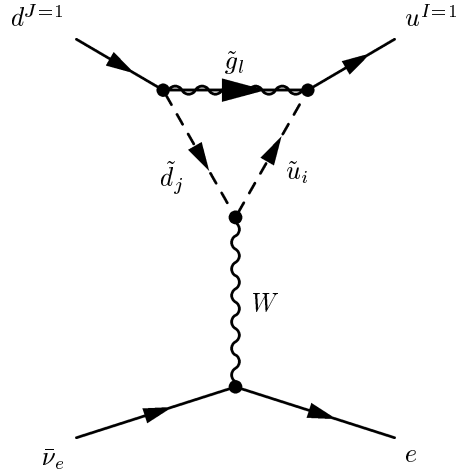


Figure 11: Vertex correction with gluino- $\tilde{u}$ - $\tilde{d}$  loop.

with

$$A_2 = g_3 \sqrt{2} Z_U^{(I+3)i} \quad (\text{B.8a})$$

$$B_2 = -g_3 \sqrt{2} Z_U^{Ii} \quad (\text{B.8b})$$

$$C_2 = -g_3 \sqrt{2} Z_D^{Jj} \quad (\text{B.8c})$$

$$D_2 = g_3 \sqrt{2} Z_D^{(J+3)j} \quad (\text{B.8d})$$

$$E_2 = Z_D^{Jj*} Z_U^{Ii*} C^{IJ} \quad (\text{B.8e})$$

**Diagram 3: Neutralino-Chargino- $\tilde{d}$  vertex correction**

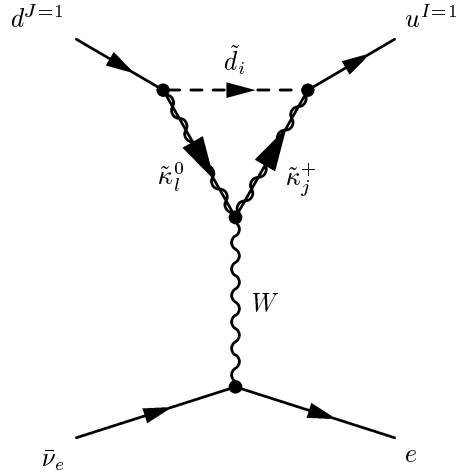


Figure 12: Vertex correction with neutralino-chargino- $\tilde{d}$  loop.

$$\begin{aligned}
\frac{d\Gamma_3}{dE_e d \cos \theta_{e\bar{\nu}}} = & \frac{d\Gamma_{\text{tree}}}{dE_e d \cos \theta_{e\bar{\nu}}} \cdot \vec{s}_n \cdot \left( \frac{\vec{p}_e \times \vec{p}_{\bar{\nu}}}{E_e E_{\bar{\nu}}} \right) \frac{1}{2m_n U^2 V^2} \frac{\Re(UV^2)}{16\pi^2} \\
& \left[ \left( -\Im(A_3 C_3 F_3) m_p \right) C_{\mu\nu}(0, 0, m_{\tilde{\kappa}_l^0}, m_{\tilde{\kappa}_j^+}, m_{\tilde{d}_i}) \delta^{\mu\nu} \right. \\
& + 2 \left( \Im(A_3 D_3 F_3) m_p m_{\tilde{\kappa}_j^+} m_{\tilde{\kappa}_l^0} C_0(0, 0, m_{\tilde{d}_i}, m_{\tilde{\kappa}_l^0}, m_{\tilde{\kappa}_j^+}) \right. \\
& + \Im(B_3 D_3 E_3) m_n^3 C_{D3}(0, 0, m_{\tilde{d}_i}, m_{\tilde{\kappa}_l^0}, m_{\tilde{\kappa}_j^+}) \\
& \left. \left. + \left( \Im(A_3 D_3 E_3) m_{\tilde{\kappa}_j^+} + \Im(B_3 D_3 F_3) m_{\tilde{\kappa}_l^0} \right) m_n^2 C_{D2}(0, 0, m_{\tilde{d}_i}, m_{\tilde{\kappa}_l^0}, m_{\tilde{\kappa}_j^+}) \right) \right] \\
& + \dots
\end{aligned} \tag{B.9}$$

with

$$A_3 = Y_u^I Z_D^{Mi*} Z_+^{2j} C^{IM} \tag{B.10a}$$

$$B_3 = - \left( \frac{e}{\sin \theta_W} Z_D^{Mi*} Z_-^{1j*} + Y_d^I Z_D^{(M+3)i*} Z_-^{2j*} \right) C^{IM} \tag{B.10b}$$

$$C_3 = \frac{e}{\sin \theta_W} \left( Z_+^{1j*} Z_N^{2l} - \frac{1}{\sqrt{2}} Z_+^{2j*} Z_N^{4l} \right) \tag{B.10c}$$

$$D_3 = \frac{e}{\sin \theta_W} \left( Z_-^{1j} Z_N^{2l*} + \frac{1}{\sqrt{2}} Z_-^{2j} Z_N^{3l*} \right) \tag{B.10d}$$

$$E_3 = \left( -\frac{e}{\sqrt{2} \sin \theta_W \cos \theta_W} Z_D^{Ji} \left( \frac{1}{3} Z_N^{1l} \sin \theta_W - Z_N^{2l} \cos \theta_W \right) + Y_d^J Z_D^{(J+3)i} Z_N^{3l} \right) \delta^{JM} \tag{B.10e}$$

$$F_3 = \left( \frac{-\sqrt{2}e}{3 \cos \theta_W} Z_D^{(J+3)i} Z_N^{1l*} + Y_d^J Z_D^{Ji} Z_N^{3l*} \right) \delta^{JM} \tag{B.10f}$$

**Diagram 4: Chargino-Neutralino- $\tilde{u}$  vertex correction**

$$\begin{aligned}
\frac{d\Gamma_4}{dE_e d \cos \theta_{e\bar{\nu}}} = & \frac{d\Gamma_{\text{tree}}}{dE_e d \cos \theta_{e\bar{\nu}}} \cdot \vec{s}_n \cdot \left( \frac{\vec{p}_e \times \vec{p}_{\bar{\nu}}}{E_e E_{\bar{\nu}}} \right) \frac{1}{2m_n U^2 V^2} \frac{\Re(UV^2)}{16\pi^2} \\
& \left[ \left( -\Im(A_4 C_4 F_4) m_p \right) C_{\mu\nu}(0, 0, m_{\tilde{\kappa}_l^-}, m_{\tilde{\kappa}_j^0}, m_{\tilde{u}_i}) \delta^{\mu\nu} \right. \\
& + 2 \left( \Im(A_4 D_4 F_4) m_p m_{\tilde{\kappa}_j^0} m_{\tilde{\kappa}_l^-} C_0(0, 0, m_{\tilde{u}_i}, m_{\tilde{\kappa}_l^-}, m_{\tilde{\kappa}_j^0}) \right. \\
& + \Im(B_4 D_4 E_4) m_n^3 C_{D3}(0, 0, m_{\tilde{u}_i}, m_{\tilde{\kappa}_l^-}, m_{\tilde{\kappa}_j^0}) \\
& \left. \left. + \left( \Im(A_4 D_4 E_4) m_{\tilde{\kappa}_j^0} + \Im(B_4 D_4 F_4) m_{\tilde{\kappa}_l^-} \right) m_n^2 C_{D2}(0, 0, m_{\tilde{u}_i}, m_{\tilde{\kappa}_l^-}, m_{\tilde{\kappa}_j^0}) \right) \right] \\
& + \dots
\end{aligned} \tag{B.11}$$

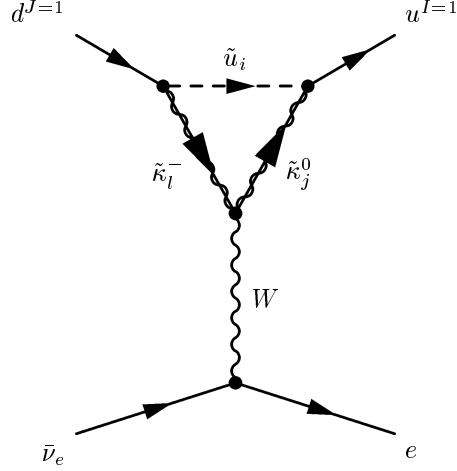


Figure 13: Vertex correction with chargino–neutralino– $\tilde{u}$  loop.

with

$$A_4 = \left( \frac{2\sqrt{2}e}{3 \cos \theta_W} Z_U^{(I+3)i} Z_N^{1j} - Y_u^I Z_U^{Ii} Z_N^{4j} \right) \delta^{IM} \quad (\text{B.12a})$$

$$B_4 = - \left[ \frac{e}{\sqrt{2} \sin \theta_W \cos \theta_W} Z_U^{Ii} \left( \frac{1}{3} Z_N^{1j*} \sin \theta_W + Z_N^{2j*} \cos \theta_W \right) + Y_u^I Z_U^{(I+3)i} Z_N^{4j*} \right] \delta^{IM} \quad (\text{B.12b})$$

$$C_4 = - \frac{e}{\sin \theta_W} \left( Z_-^{1l} Z_N^{2j*} + \frac{1}{\sqrt{2}} Z_-^{2l} Z_N^{3j*} \right) \quad (\text{B.12c})$$

$$D_4 = \frac{e}{\sin \theta_W} \left( -Z_+^{1l*} Z_N^{2j} + \frac{1}{\sqrt{2}} Z_+^{2l*} Z_N^{4j} \right) \quad (\text{B.12d})$$

$$E_4 = \left( -\frac{e}{\sin \theta_W} Z_U^{Mi*} Z_+^{1l} + Y_u^M Z_U^{(M+3)i*} Z_+^{2l} \right) C^{MJ} \quad (\text{B.12e})$$

$$F_4 = - Y_d^J Z_U^{Mi*} Z_-^{2l*} C^{MJ} \quad (\text{B.12f})$$

**Diagram 5: Box with  $\tilde{u}$**

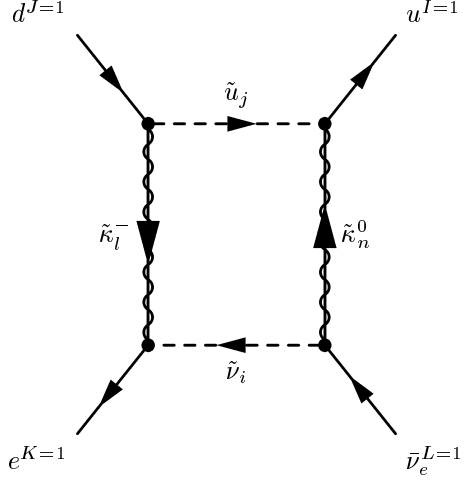


Figure 14: Box diagram with  $\tilde{u}$  in the loop.

$$\begin{aligned}
\frac{d\Gamma_5}{dE_e d \cos \theta_{e\bar{\nu}}} = & \frac{d\Gamma_{\text{tree}}}{dE_e d \cos \theta_{e\bar{\nu}}} \cdot \vec{s}_n \cdot \left( \frac{\vec{p}_e \times \vec{p}_{\bar{\nu}}}{E_e E_{\bar{\nu}}} \right) \frac{m_W^2}{4m_n U^2 V^2} \frac{\Re(UV)}{16\pi^2} \\
& \left\{ \left( \Im(A_5 D_5 F_5 G_5) m_e \right) D_{\mu\nu}(0, 0, 0, m_{\tilde{u}_j}, m_{\tilde{\nu}_i}, m_{\tilde{\kappa}_n^0}, m_{\tilde{\kappa}_l^-}) \delta^{\mu\nu} \right. \\
& + 2 \left[ \Im(B_5 D_5 E_5 G_5) m_p m_{\tilde{\kappa}_l^-} m_{\tilde{\kappa}_n^0} D_0(0, 0, 0, m_{\tilde{\kappa}_l^-}, m_{\tilde{u}_j}, m_{\tilde{\nu}_i}, m_{\tilde{\kappa}_n^0}) \right. \\
& + \left( \Im(B_5 D_5 F_5 G_5) m_{\tilde{\kappa}_l^-} m_n^2 + \Im(B_5 C_5 E_5 G_5) m_{\tilde{\kappa}_n^0} m_n^2 \right) \\
& \quad D_{D1}(0, 0, 0, m_{\tilde{\kappa}_l^-}, m_{\tilde{u}_j}, m_{\tilde{\nu}_i}, m_{\tilde{\kappa}_n^0}) \\
& \quad \left. + \Im(B_5 C_5 F_5 G_5) m_n^3 D_{D2}(0, 0, 0, m_{\tilde{\kappa}_l^-}, m_{\tilde{u}_j}, m_{\tilde{\nu}_i}, m_{\tilde{\kappa}_n^0}) \right] \} \\
& + \dots
\end{aligned} \tag{B.13}$$

with

$$A_5 = -Y_l^K Z_\nu^{Ki} Z_-^{2l-} \quad (\text{B.14a})$$

$$B_5 = -\frac{e}{\sin \theta_W} Z_\nu^{Ki} Z_+^{1l*} \quad (\text{B.14b})$$

$$C_5 = -\left(\frac{e}{\sin \theta_W} Z_U^{Mj*} Z_+^{1l} + Y_u^M Z_U^{(M+3)j*} Z_+^{2l}\right) C^{MJ} \quad (\text{B.14c})$$

$$D_5 = -Y_d^J Z_U^{Mj*} Z_-^{2l*} C^{MJ} \quad (\text{B.14d})$$

$$E_5 = \left(\frac{2\sqrt{2}e}{3 \cos \theta_W} Z_U^{(I+3)j} Z_N^{1n} - Y_u^I Z_N^{4n} Z_U^{Ij}\right) \delta^{MI} \quad (\text{B.14e})$$

$$F_5 = \left[-\frac{e}{\sqrt{2} \sin \theta \cos \theta_W} Z_U^{Ij} \left(\frac{1}{3} Z_N^{1n*} \sin \theta + Z_N^{2n*} \cos \theta\right) - Y_u^I Z_N^{4n*} Z_U^{(I+3)j}\right] \delta^{MI} \quad (\text{B.14f})$$

$$G_5 = \frac{e}{\sqrt{2} \sin \theta \cos \theta_W} Z_\nu^{Li*} (Z_N^{1n} \sin \theta - Z_N^{2n} \cos \theta) \quad (\text{B.14g})$$

**Diagram 6: Box with  $\tilde{d}$**

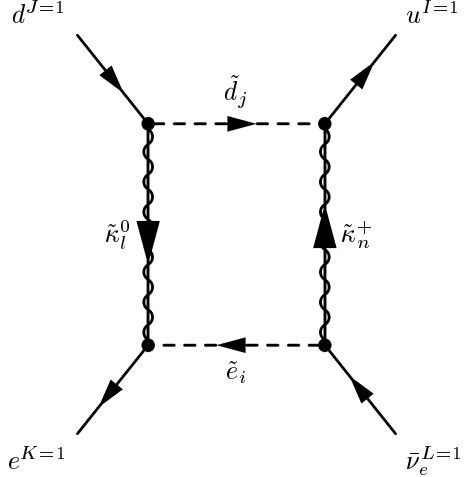


Figure 15: Box diagram with  $\tilde{d}$  in the loop.

$$\begin{aligned}
\frac{d\Gamma_6}{dE_e d\cos\theta_{e\bar{\nu}}} = & \frac{d\Gamma_{\text{tree}}}{dE_e d\cos\theta_{e\bar{\nu}}} \cdot \vec{s}_n \cdot \left( \frac{\vec{p}_e \times \vec{p}_{\bar{\nu}}}{E_e E_{\bar{\nu}}} \right) \frac{m_W^2}{4m_n U^2 V^2} \frac{\Re(UV)}{16\pi^2} \\
& \left\{ \left( \Im(A_6 D_6 F_6 G_6) m_e \right) D_{\mu\nu}(0, 0, 0, m_{\tilde{d}_j}, m_{\tilde{e}_i}, m_{\tilde{\kappa}_n^+}, m_{\tilde{\kappa}_l^0}) \delta^{\mu\nu} \right. \\
& + 2 \left[ \Im(B_6 D_6 E_6 G_6) m_p m_{\tilde{\kappa}_l^0} m_{\tilde{\kappa}_n^+} D_0(0, 0, 0, m_{\tilde{\kappa}_l^0}, m_{\tilde{d}_j}, m_{\tilde{e}_i}, m_{\tilde{\kappa}_n^+}) \right. \\
& + \left( \Im(B_6 D_6 F_6 G_6) m_{\tilde{\kappa}_l^0} m_n^2 + \Im(B_6 C_6 E_6 G_6) m_{\tilde{\kappa}_n^+} m_n^2 \right) \\
& D_{D1}(0, 0, 0, m_{\tilde{\kappa}_l^0}, m_{\tilde{d}_j}, m_{\tilde{e}_i}, m_{\tilde{\kappa}_n^+}) \\
& \left. + \Im(B_6 C_6 F_6 G_6) m_n^3 D_{D2}(0, 0, 0, m_{\tilde{\kappa}_l^0}, m_{\tilde{d}_j}, m_{\tilde{e}_i}, m_{\tilde{\kappa}_n^+}) \right] \left. \right\} \\
& + \dots
\end{aligned} \tag{B.15}$$

with

$$A_6 = -\frac{\sqrt{2}e}{\cos\theta_W} Z_L^{(K+3)i*} Z_N^{1l} + Y_l^K Z_N^{3l} Z_L^{Ki*} \tag{B.16a}$$

$$B_6 = \frac{e}{\sqrt{2}\sin\theta\cos\theta_W} Z_L^{Ki*} (Z_N^{1l*} \sin\theta + Z_N^{2l*} \cos\theta) + Y_l^K Z_N^{3l*} Z_L^{(K+3)i*} \tag{B.16b}$$

$$C_6 = \left( \frac{-e}{\sqrt{2}\sin\theta\cos\theta_W} Z_D^{Jj} \left( \frac{1}{3} Z_N^{1l} \sin\theta - Z_N^{2l} \cos\theta \right) + Y_d^J Z_D^{(J+3)j} Z_N^{3l} \right) \delta^{MJ} \tag{B.16c}$$

$$D_6 = \left( -\frac{\sqrt{2}e}{3\cos\theta_W} Z_D^{(J+3)j} Z_N^{1l*} + Y_d^J Z_N^{3l*} Z_D^{Jj} \right) \delta^{MJ} \tag{B.16d}$$

$$E_6 = -Y_u^M Z_D^{Ij*} Z_+^{2n} C^{IM} \tag{B.16e}$$

$$F_6 = -\left( \frac{e}{\sin\theta_W} Z_D^{Ij*} Z_-^{1n*} + Y_d^I Z_D^{(I+3)j} Z_-^{2n*} \right) C^{IM} \tag{B.16f}$$

$$G_6 = -\left( \frac{e}{\sin\theta_W} Z_L^{Li} Z_-^{1n} + Y_l^L Z_L^{(L+3)i} Z_-^{2n} \right) \tag{B.16g}$$

## C Loop Integrals

In this Appendix we have summarized the definitions of the loop integrals which were used in the calculation of the Feynman diagrams in the previous Appendix.

### C.1 2-point Functions

First we define the 2-point functions as in [15] because most 3- and 4-point functions will be expressed in terms of these.

$$B_0(q^2, m_1, m_2) = \Delta - \int_0^1 dx \ln H \quad (C.1)$$

$$B_1(q^2, m_1, m_2) = -\frac{1}{2}\Delta + \int_0^1 dx x \ln H \quad (C.2)$$

$$B_{21}(q^2, m_1, m_2) = \frac{1}{3}\Delta - \int_0^1 dx x^2 \ln H \quad (C.3)$$

$$\begin{aligned} B_3(q^2, m_1, m_2) &= -B_1(q^2, m_1, m_2) - B_{21}(q^2, m_1, m_2) \\ &= \frac{1}{6}\Delta - \int_0^1 dx x(1-x) \ln H \end{aligned} \quad (C.4)$$

with

$$H = [(1-x)m_1^2 + xm_2^2 - x(1-x)q^2 - i\epsilon] \quad (C.5)$$

$$\Delta = \frac{1}{\epsilon} - \gamma_E + \ln 4\pi \quad (C.6)$$

where  $\gamma_E = -\frac{d \ln \Gamma(x)}{dx} \Big|_{x=1} = 0,577216\dots$  denotes the Euler constant. Since the one-loop corrections to  $D$  are finite, the terms  $\propto \Delta$  cancel in the combinations of  $B$ -functions that will appear below.

## C.2 3-point Functions

Besides the standard integrals  $C_0$  and  $C_{\mu\nu}$  with vanishing external momenta, we need the following integrals which contain combinations of the Feynman parameters in the nominator.

$$\begin{aligned} C_{D1}(0, 0, m_1, m_2, m_3) &= \int_0^1 dx \int_0^{1-x} dy \frac{x+y}{m_1^2(1-x-y) + m_2^2x + m_3^2y} \\ &= \frac{1}{m_3^2 - m_2^2} (B_0(0, m_2, m_1) - B_0(0, m_3, m_1) - B_1(0, m_2, m_1) + B_1(0, m_3, m_1)) \end{aligned} \quad (C.7)$$

$$\begin{aligned} C_{D2}(0, 0, m_1, m_2, m_3) &= \int_0^1 dx \int_0^{1-x} dy \frac{1-x-y}{m_1^2(1-x-y) + m_2^2x + m_3^2y} \\ &= \frac{1}{m_3^2 - m_2^2} (B_1(0, m_2, m_1) - B_1(0, m_3, m_1)) \end{aligned} \quad (C.8)$$

$$\begin{aligned} C_{D3}(0, 0, m_1, m_2, m_3) &= \int_0^1 dx \int_0^{1-x} dy \frac{(1-x-y)^2}{m_1^2(1-x-y) + m_2^2x + m_3^2y} \\ &= \frac{1}{m_3^2 - m_2^2} (B_1(0, m_2, m_1) - B_1(0, m_3, m_1) - B_3(0, m_2, m_1) + B_3(0, m_3, m_1)) \end{aligned} \quad (C.9)$$

### C.3 4-point Functions

Here the standard integrals  $D_0$  and  $D_{\mu\nu}$  with vanishing external momenta are needed. In addition the following two integrals with Feynman parameters appear:

$$\begin{aligned}
D_{D1}(0, 0, 0, m_1, m_2, m_3, m_4) &= \int_0^1 dx \int_0^{1-x} dy \int_0^{1-x-y} dz \frac{x}{[m_1^2(1-x-y-z) + m_2^2x + m_3^2y + m_4^2z]^2} \\
&= \frac{1}{m_4^2 - m_1^2} \left( \frac{1}{m_3^2 - m_4^2} (B_1(0, m_3, m_2) - B_1(0, m_4, m_2)) \right. \\
&\quad \left. - \frac{1}{m_3^2 - m_1^2} (B_1(0, m_3, m_2) - B_1(0, m_1, m_2)) \right) \tag{C.10}
\end{aligned}$$

$$\begin{aligned}
D_{D2}(0, 0, 0, m_1, m_2, m_3, m_4) &= \int_0^1 dx \int_0^{1-x} dy \int_0^{1-x-y} dz \frac{x^2}{[m_1^2(1-x-y-z) + m_2^2x + m_3^2y + m_4^2z]^2} \\
&= \frac{1}{m_4^2 - m_1^2} \left( \frac{1}{m_3^2 - m_4^2} (B_1(0, m_3, m_2) - B_1(0, m_4, m_2) \right. \\
&\quad \left. - B_3(0, m_3, m_2) + B_3(0, m_4, m_2)) \right. \\
&\quad \left. - \frac{1}{m_3^2 - m_1^2} (B_1(0, m_3, m_2) - B_1(0, m_1, m_2) \right. \\
&\quad \left. - B_3(0, m_3, m_2) + B_3(0, m_1, m_2)) \right) \tag{C.11}
\end{aligned}$$

## References

- [1] E. Christova and M. Fabbrichesi, Phys. Lett. **B315** (1993) 113, hep-ph/9302303.
- [2] J. Rosiek, hep-ph/9511250.
- [3] P. Herczeg and I.B. Khriplovich, Phys. Rev. **D56** (1997) 80.
- [4] T. Soldner, PhD thesis, TU München (2001); see also the TRINE home page, <http://www1.physik.tu-muenchen.de/~tsoldner/trine/> .
- [5] C.G. Jr. Callan and S.B. Treiman, Phys. Rev. **162** (1967) 1494.
- [6] Particle Data Group, K. Hagiwara et al., Phys. Rev. **D66** (2002) 010001.
- [7] H. Georgi and L. Randall, Nucl. Phys. **B276** (1986) 241.
- [8] T. Ibrahim and P. Nath, Phys. Rev. **D57** (1998) 478, Erratum-ibid. **D58** (1998), **D60**, (1999) 019901], hep-ph/9708456; M. Brhlik, G.J. Good and G.L. Kane, Phys. Rev. **D59** (1999) 115004, hep-ph/9810457.
- [9] F. Gabbiani, E. Gabrielli, A. Masiero and L. Silvestrini, Nucl. Phys. **B477** (1996) 321.
- [10] U. Ellwanger, Phys. Lett. **B141** (1984) 435.
- [11] R.M. Godbole, S. Pakvasa, S.D. Rindani and X. Tata, Phys. Rev. **D61** (2000) 113003, hep-ph/9912315; S.A. Abel, A. Dedes and H.K. Dreiner, JHEP **0005** (2000) 013, hep-ph/9912429.
- [12] A. Bartl, E. Christova and W. Majerotto, Nucl. Phys. **B460** (1996) 235, Erratum-ibid. **B465** (1996) 365, hep-ph/9507445.
- [13] J. Liu, Phys. Rev. **D48** (1993) 212, hep-ph/9207271.
- [14] J.A. Vermaseren, KEK-TH-326, and math-ph/0010025.
- [15] G. Passarino and M. J. Veltman, Nucl. Phys. **B160** (1979) 151.